RESEARCH ARTICLE | APRIL 01 2024

A reexamination of the Cox–Merz rule through the lens of recovery rheology

Yul Hui Shim (10); James J. Griebler (10); Simon A. Rogers ■ (10)



J. Rheol. 68, 381-396 (2024)

https://doi.org/10.1122/8.0000811







Advance your science, career and community as a member of The Society of Rheology







A reexamination of the Cox-Merz rule through the lens of recovery rheology

Yul Hui Shim, James J. Griebler, and Simon A. Rogers^{a)}

Department of Chemical and Biomolecular Engineering, University of Illinois at Urbana-Champaign, Urbana, Illinois 61801

(Received 21 December 2023; final revision received 25 February 2024; published 1 April 2024)

Abstract

Empirical rules play a crucial role in industrial and experimental settings for efficiently determining the rheological properties of materials, thereby saving both time and resources. An example is the Cox-Merz rule, which equates the steady-shear viscosity with the magnitude of the complex viscosity obtained in oscillatory tests. This empirical rule provides access to the steady-shear viscosity that is useful for processing conditions without the instabilities associated with experiments at high shear rates. However, the Cox-Merz rule is empirical and has been shown to work in some cases and fail in others. The underlying connection between the different material functions remains phenomenological and the lack of a comprehensive understanding of the rheological physics allows for ambiguity to persist in the interpretation of material responses. In this work, we revisit the Cox-Merz rule using recovery rheology, which decomposes the strain into recoverable and unrecoverable components. When viewed through the lens of recovery rheology, it is clearly seen that the steady-shear viscosity comes from purely unrecoverable acquisition of strain, while the complex viscosity is defined in terms of contributions from both recoverable and unrecoverable components. With recovery tests in mind, we elucidate why the Cox-Merz rule works only in a limited set of conditions and present an approach that could allow for universal comparisons to be made. This work further highlights the significance of recovery rheology by showing how it is possible to extend beyond phenomenological approaches through clear rheophysical metrics obtained by decomposing the material response into recoverable and unrecoverable components.© 2024 Published under an exclusive license by Society of Rheology. https://doi.org/10.1122/8.0000811

I. INTRODUCTION

Efforts to generally interpret a material's shear rheology have been conducted with various experimental protocols such as oscillatory, start-up, creep, and flow cessation tests. Each protocol provides various material functions such as the steady shear viscosity, the complex viscosity, and the stress growth coefficient. There are several significant empirical rules dealing with the relationships between these material functions. These empirical rules are useful both industrially and experimentally because they provide information for designing materials and their processing conditions. Among the most widely used empirical rules is the Cox-Merz rule, which was proposed in 1958 [1] and links the steady shear and oscillatory shearing responses.

The Cox-Merz rule, as indicated in Fig. 1, is an equality between the steady shear viscosity, $\eta_{ss}(\dot{\gamma})$, and the magnitude of the complex viscosity, $|\eta^*(\omega)|$ [1], when the angular frequency, ω , is numerically the same as the shear rate, $\dot{\gamma}$,

$$|\eta^*(\omega)|_{\omega=\dot{\gamma}}=\eta_{ss}(\dot{\gamma}). \tag{1}$$

The steady shear viscosity is determined by imposing a constant stress or constant shear rate and taking the ratio of stress to shear rate once all transience has died away. For example, in the start-up of the shear test, the stress growth

coefficient is defined as

$$\eta^{+}(t,\dot{\gamma}) = \frac{\sigma^{+}(t,\dot{\gamma})}{\dot{\gamma}(t)}, \qquad (2)$$

where $\sigma^+(t)$ is the shear stress growth function. From the stress growth coefficient, the steady-shear viscosity is determined when the material reaches a steady state exhibiting a constant stress

$$\eta_{ss}(\dot{\gamma}) = \frac{\sigma^{+}(t = \infty, \dot{\gamma})}{\dot{\gamma}(t)} = \frac{\sigma_{ss}(\dot{\gamma})}{\dot{\gamma}} \ . \tag{3}$$

In contrast, the magnitude of the complex viscosity is determined from oscillatory tests and is defined as the ratio of the stress amplitude to the strain rate amplitude [1,2]. It can be expressed in terms of the components of the complex viscosity or complex modulus,

$$|\eta^*| = \frac{\sigma_0}{\dot{\gamma}_0} = \sqrt{(\eta')^2 + (\eta'')^2} = \frac{\sqrt{G'^2 + G''^2}}{\omega},$$
 (4)

where σ_0 and $\dot{\gamma}_0$ are the amplitudes of the stress and strain rate, η' and η'' are the real and imaginary parts of the complex viscosity, G' is the storage modulus, G'' is the loss modulus, and ω is the angular frequency. In general, the oscillatory functions are frequency dependent, though we have neglected this functional dependence for clarity.

^{a)}Author to whom correspondence should be addressed; electronic mail: sarogers@illinois.edu

Cox-Merz Rule $|\eta^*(\omega)|_{\omega=\dot{\gamma}}=\eta(\dot{\gamma})$ $= \widehat{\Xi}$ $\text{Shear rate, } \dot{\gamma}$

FIG. 1. Cox–Merz rule proposed the equality between the magnitude of the complex viscosity $(|\eta^*(\omega)|)$ and the steady shear viscosity $(\eta(\dot{\gamma}))$ when the angular frequency is the same as the shear rate.

The Cox-Merz equality between steady and oscillatory shear has been cited over 2000 times in the last 65 years and has been reported to work with many polymeric melts [3–7] and concentrated polymer solutions [8–10] with a wide range of chemical structures and molecular weights [11-15]. The advantage of the Cox-Merz rule is that it provides a method for predicting the steady-shear viscosity, which is useful for real-world processing, from a small amplitude oscillatory shear (SAOS) test. It is, therefore, a connection between linear and nonlinear measurements. This approach allows researchers to avoid edge fracture or other instabilities that may be observed in steady-shearing experiments at high rates. While the Cox-Merz rule has been widely used [1,16–18] and modified to work for various materials [13,19–27], this empirical rule often fails for complex fluids that exhibit shear-dependent alignment such as associating polymers, liquid crystals, and anisotropic colloids [28-33], and thixotropic or yielding behaviors observed in highly concentrated suspensions, hydrogels, and polymer composites [34–36].

A modification of the Cox-Merz rule designed for use in the study of yield stress fluids is referred to as the Rutgers-Delaware rule [19]. Doraiswamy *et al.* reported that the steady-shear viscosity of a yield stress fluid equals the magnitude of the complex viscosity when the amplitude of the shear rate in the oscillatory test is equal to the steady shear rate in a sample that has yielded. The Rutgers-Delaware rule (or modified Cox-Merz rule) is not intended to work when the strain is too small to yield the material.

The validity of the Cox-Merz rule depends on the shear rates and materials being tested [28–40]. When the Cox-Merz rule fails, the magnitude of the complex viscosity can be larger than the steady-shear viscosity [13] or vice versa [41]. Attempts have been made to explain why the Cox-Merz rule fails. In terms of particle microstructure, failure has been described as particle diffusion due to hydrodynamics and interparticle interactions [42,43], particle migration and reorganization [44,45] due to the chaotic nature of the hydrodynamic interactions [46,47], particle self-

diffusion [48], or particle collisions [49]. Nevertheless, there is a lack of a universal interpretation that can account for all material behaviors. The lack of a rheophysical understanding of when the Cox-Merz rule applies and does not apply leads to a degree of ambiguity of interpretation. Understanding why this empirical rule works under limited conditions and then finding universal relationships between different test results would remove much of this ambiguity. Rathinaraj et al. recently reported why the Cox-Merz rule works under specific conditions from a mathematical point of view [50,51]. They showed that the Cox-Merz rule is mathematically satisfied for materials with broad relaxation spectra and sufficiently strong strain-dependent damping, implying that the underlying physics could be explored experimentally. Their mathematical expression was illustrated using experimental measurements with one specific material which is well described by the assumed framework. While Rathinaraj et al. positioned their study as exploring what constitutive behaviors are required for the Cox-Merz rule to work, we explore the possibility in this work that a rephrasing of the Cox-Merz rule, taking measurable rheophysical concepts into account, could lead to a more general equating of a steady-shear and oscillatory measures that is agnostic to particular features of constitutive behaviors.

A recently introduced experimental technique, called recovery rheology [52–63], starts from the decomposition of strain, γ , into recoverable and unrecoverable components,

$$\gamma(t) = \gamma_{rec}(t) + \gamma_{un}(t). \tag{5}$$

Traditional material functions derived from the total strain or total strain rate are, therefore, composite parameters.

In recovery rheology, the recoverable and unrecoverable components are interpreted as being associated with viscoelastic solid and plastic (or fluid) properties under shear [55–58], respectively. While similar language is used, these ideas are distinct from how much material properties recover after the imposition of a large deformation in the three-interval thixotropy test (3ITT), which is often also called recovery.

By experimentally decomposing strains and strain rates into recoverable and unrecoverable components, recovery rheology has begun to provide a clear understanding of rheological phenomena from an energetic perspective. The studies of Donley *et al.* [55] and others [56–58] have reported that the dynamic loss modulus, G'', traditionally considered a singular viscous modulus, is related to the average energy dissipated during an oscillation [64],

$$G''(\omega) = \frac{2(\dot{W}_{diss}(\omega))_{avg}}{\gamma_0^2 \omega} = \frac{2[\sigma(t)\dot{\gamma}(t)]_{avg}}{\gamma_0^2 \omega},$$
 (6)

and is a composite parameter that can be decomposed into contributions dependent on the rate of acquisition of recoverable and unrecoverable strains. The loss modulus, therefore, can be defined as a sum of two terms in recovery rheology, one each from solidlike and fluidlike components of energy

21 May 2024 16:1

dissipation

$$G''_{solid}(\omega) = \frac{2(\dot{W}_{diss,solid}(\omega))_{avg}}{\gamma_0^2 \omega} = \frac{2[\sigma(t)\dot{\gamma}_{rec}(t)]_{avg}}{\gamma_0^2 \omega}, \quad (7)$$

$$G''_{fluid}(\omega) = \frac{2(\dot{W}_{diss,fluid}(\omega))_{avg}}{\gamma_0^2 \omega} = \frac{2[\sigma(t)\dot{\gamma}_{un}(t)]_{avg}}{\gamma_0^2 \omega}.$$
 (8)

Since the strain rate is a sum of recoverable and unrecoverable strain rates, the energy terms are too,

$$G''(\omega) = G''_{solid}(\omega) + G''_{fluid}(\omega). \tag{9}$$

The Cox-Merz rule is equivalence between viscosities obtained from different protocols. By acknowledging the distinct nature of recoverable and unrecoverable strains and rates, Singh et al. [63] showed that two viscosities can be defined for an arbitrary experiment. One viscosity is related to the rate at which strain is acquired recoverably, and one related to the rate at which strain is acquired unrecoverably. Given the clear connection between strain acquisition modes and the behaviors of the Kelvin-Voigt and Maxwell viscoelastic models, we refer to the two viscosities as the retardation viscosity and the flow viscosity, $\eta_{ret}(t) = \sigma(t)/\dot{\gamma}_{rec}(t)$ and $\eta_{flow}(t) = \sigma(t)/\dot{\gamma}_{un}(t)$. In shear start-up tests, Singh *et al.* showed that the stress growth coefficient, defined as the ratio of the shear stress to the total rate, $\eta^+(t) = \sigma^+(t)/\dot{\gamma}(t)$, is also a composite parameter and can be decomposed into recoverable and unrecoverable components. In the following year, Griebler et al. [57] showed that the steady shear viscosity equals the energy dissipation term normalized by the unrecoverable strain during oscillation, implying that the steady shear viscosity is associated with the acquisition of unrecoverable strain.

In this work, we reexamine the Cox-Merz rule through the lens of recovery rheology. We study a variety of model systems, one of which is polystyrene (PS), which was the original material used in the first report of the Cox-Merz rule [1]. Additionally, we have studied an entangled selfassembled surfactant solution, a hydrogel that exhibits shearthickening behavior, a graphene oxide (GO) suspension, a branched polymer system, and a model lithium-ion battery anode slurry. The paper is laid out as follows. In Sec. II, we introduce recovery rheology and the experimental techniques, showing how the material functions can be obtained. In Sec. III, we describe the sample preparation and the details of the recovery rheology test including the iterative recovery test and strain shift test. In Sec. IV, we show the experimental measurements obtained from PS. The traditional rheological characterizations including a measurement of the steadyshear flow curve and frequency sweeps are presented in Sec. IV A. In Sec. IV B, the transient flow behavior and the oscillatory sweep test are examined through the lens of recovery rheology. In Sec. IV C, we show how the rheological physics behind the Cox-Merz rule can be understood and how a comparison of flow viscosities can be used to predict the steady shear viscosity in a potentially universal way.

II. RECOVERY RHEOLOGY METRICS

A. Material functions and recovery rheology

Prior to revisiting the Cox–Merz, it is important to be clear about the material functions included in each empirical rule. In this section, we examine the stress growth coefficient, the steady shear viscosity, and the complex viscosity through the lens of recovery rheology. Traditional rheology uses one strain component, referred to here as the total strain, while recovery rheology sees strain as a composite parameter made of the recoverable and unrecoverable components as in Eq. (5). Recovery rheology, therefore, allows for the decomposition of material functions into recoverable and unrecoverable components.

The complex viscosity is a complex function describing the ratio of the oscillatory stress to the oscillatory strain rate. It consists of real and imaginary components, η' and η'' , and its magnitude is related to the dynamic moduli, G'' and G', as shown in Eq. (4). Considering that G'' is a sum of recoverable and unrecoverable terms, G''_{solid} and G''_{fluid} , the magnitude of the complex viscosity can be expressed as

$$|\eta^*(\omega)| = \sqrt{G'^2 + \left(G''_{solid} + G''_{fluid}\right)^2} / \omega$$
. (10)

The dynamic viscosity, $\eta' = G''/\omega = (G''_{solid} + G''_{fluid})/\omega$, is, therefore, also related to both recoverable and unrecoverable strain rates.

The stress growth coefficient defined in Eq. (2) can be described in terms of the recoverable and unrecoverable components of the strain rate

$$\eta^{+}(t) = \frac{\sigma(t)}{\dot{\gamma}_{tot}(t)} = \frac{\sigma(t)}{\dot{\gamma}_{rec}(t) + \dot{\gamma}_{un}(t)} . \tag{11}$$

Decomposing the total strain rate into components, therefore, allows material functions to be defined in terms of the retardation viscosity and flow viscosity [63]. The flow viscosity is defined only in terms of the unrecoverable strain rate as

$$\eta_{flow}(t) = \frac{\sigma(t)}{\dot{\gamma}_{un}(t)} \ . \tag{12}$$

The steady shear viscosity obtained when all transience has died away will be the same whether Eq. (11) or Eq. (12) is used because the recoverable strain saturates at a steady state. The recoverable strain rate is, therefore, zero at a steady state, and the steady shear viscosity comes from purely unrecoverable deformation. The steady-shear viscosity, the stress growth coefficient, and the flow viscosity are, therefore, equal at the steady state.

The Cox–Merz rule provides a way to predict the steady shear viscosity from the magnitude of the complex viscosity, $|\eta^*(\omega)|$, or the dynamic viscosity, η' . However, the complex viscosity and the dynamic viscosity contain both recoverable and unrecoverable components, while the steady shear viscosity comes from the unrecoverable response only. This

21 May 2024 16:19:53

implies that the traditional formulation of the Cox–Merz rule should work when the recoverable response to oscillatory shearing is small enough to be ignored, or when the unrecoverable response is dominant.

To predict the steady shear viscosity from the oscillatory shear test in a general case, it is, therefore, necessary to extract the unrecoverable response from the complex viscosity.

The time-resolved flow viscosity is defined in terms of the unrecoverable strain rate alone, as shown in Eq. (12). An average flow viscosity can similarly be defined from the oscillatory shear test in terms of an unrecoverable parameter. Griebler *et al.* [57] proposed the dynamic flow viscosity as

$$\eta_{flow}(\omega) = \frac{G''_{fluid,raw}}{\omega} = \frac{2[\sigma(t)\dot{\gamma}_{un}(t)]_{avg}}{\omega\gamma_{0um}^2} \ . \tag{13}$$

The dynamic flow viscosity in Eq. (13) can be calculated from data obtained in iterative recovery tests that provide the time-resolved stress and strain components.

A new experiment that has come from studying recovery rheology, called the strain shift test, also allows for a simple determination of the flow viscosity. When a phase-shifted oscillatory stress, $\sigma(t) = \sigma_0 \sin(\omega t + \psi)$, is imposed, the resulting strain response oscillates about a nonzero value called the strain shift. The strain shift, γ_s , is attributed to the acquisition of unrecoverable strain only [52,62] and, therefore, allows for a determination of the flow viscosity

$$\eta_{flow}(\omega) = \frac{\sigma_0}{\omega \gamma_s \cos(\psi)}$$
 (14)

As $\omega \gamma_0$ represents the strain rate, $\omega \gamma_s$ is equal to the unrecoverable strain rate. For simplicity, we use sinusoidal stresses, so that $\psi = 0$ and the strain shift is maximized. Details for this derivation are in Appendix A.

As shown in Eqs. (10) and (11), the stress growth coefficient and the complex viscosity reflect both recoverable and unrecoverable responses, indicating that the two material functions are composite parameters. In contrast, recovery rheology allows us to isolate the unrecoverable response as shown in Eqs. (12)–(14).

B. Relations between material functions

The magnitude of the complex viscosity is equal to the magnitude of the complex modulus, $|G^*|$, divided by the angular frequency, $|\eta^*| = |G^*|/\omega = \sqrt{G'^2 + G''^2}/\omega$. A simple expression of the magnitude of the complex viscosity is, therefore,

$$|\eta^*| = \sqrt{\frac{G'^2 + G''^2}{\omega}} = \frac{\sigma_0}{\gamma_0 \omega} \ .$$
 (15)

The unrecoverable flow viscosity can be rewritten as

$$\eta_{flow} = \frac{G''_{fluid,raw}}{\omega} = \frac{\sigma_0}{\omega \gamma_s \cos(\psi)} = \frac{\sigma_0}{\omega \gamma_s}, \quad (16)$$

where ψ is the phase angle of the applied stress wave and $\cos(\psi) = 1$ when a sinusoidal stress is applied [62]. Since the magnitude of the complex viscosity is $\sigma_0/\omega\gamma_0$, it can be transformed to the flow viscosity by multiplying by the ratio of the total strain and the strain shift

$$|\eta^*| \frac{\gamma_0}{\gamma_s} = \left(\frac{\sigma_0}{\omega \gamma_0}\right) \left(\frac{\gamma_0}{\gamma_s}\right) = \frac{\sigma_0}{\omega \gamma_s} = \eta_{flow.}$$
 (17)

Therefore, a measurement of the strain shift, γ_s , can be used to calculate the unrecoverable flow viscosity.

The comparison of the expressions for the magnitude of the complex viscosity and the flow viscosity implies that the Cox–Merz rule works when the strain shift, γ_s , which is a measure of the unrecoverable strain amplitude, is approximately equal to the total strain ($\gamma_0 \approx \gamma_s = \gamma_{un,0}$). This is equivalent to saying the Cox–Merz rule works when any recoverable contribution to G" and η' is small, or when most of the strain is acquired unrecoverably. Furthermore, this line of reasoning allows us to explain why the Rutgers–Delaware rule works only when the sample is yielded [19]. In the yielded state most of the strain is acquired unrecoverably [57]. Thus, the magnitude of the complex viscosity at a rate amplitude $\omega\gamma_0$ reflects the unrecoverable deformation, just as the steady-shear viscosity does.

III. MATERIAL AND METHODS

A. Material preparation

PS was purchased from Sigma-Aldrich with $^{\frac{50}{20}}$ $M_w = 192\,000\,\text{g/mol}$ and a softening point = $107\,^{\circ}\text{C}$. PS $^{\frac{50}{20}}$ samples were prepared as disk-shape pellets by a hot-press at $^{\frac{50}{20}}$ °C. The pellets were 1 mm thick with diameters of 25 mm. The rheological properties were measured with a plate-plate geometry of diameter 25 mm. To minimize oxidation of polymer at a high temperature ($130-190\,^{\circ}\text{C}$), all tests were carried out while flowing N_2 gas.

The polyvinyl alcohol (PVA)-borax hydrogel was prepared by mixing PVA of M_w 85 k-124 kg/mol, purchased from Sigma-Aldrich, and sodium tetraborate (Borax, Na₂B₄O₇). For mixing, two stock solutions were prepared: PVA was dissolved in de-ionized water at 4 wt. % concentration by magnetically stirring at 300 rpm at 95 °C overnight, while a borax solution of 4 wt. % was also prepared by stirring under the same stirring speed and temperature for 4 h. The two stock solutions were then left at room temperature for about a day and then poured into a centrifuge tube to form a cross-linked PVA-borax hydrogel with a ratio of PVA and borax solution of 2.75:1.75. The centrifuge tube containing the mixture with the desired amount of the two stock solutions was thoroughly shaken until the mixture showed a clear transparent hydrogel. The hydrogel was allowed to rest for a day for a complete cross-linked gel. The PVA-borax hydrogel was then centrifuged at 3000 rpm for 10 min and this step was repeated until the trapped air bubbles in the hydrogel were fully removed. The rheological properties were measured with a cone-plate geometry of diameter 50 mm and angle 2° at 25 °C.

21 May 2024 16:19:53

The GO suspension was supplied from STANDARD GRAPHENE. The concentration of the GO stock suspension dispersed the de-ionized water is 1 wt. %. The GO has a lateral dimension of 8 µm with an approximate thickness of 1 nm. The GO stock suspension is used as a model system of anisotropic colloids and liquid crystal colloids. The rheological properties were measured with a cone-plate geometry (diameter 50 mm, angle 1°) at 20 °C.

The composite of graphite-carbon black-polymer binder (Gr-CB-CMC composite) is used as a model system of the lithium-ion battery anode slurry. The graphite was supplied from Sigma-Aldrich. The graphite has a 20 µm diameter, a density of 2.26 g/cm³, and molecular weight of 12.011 g/mol. Carbon black with a density of 1.6 g/cm³ and specific surface area of 62 m²/g was supplied from MTI Korea (Super C65). As a polymeric binder, we used sodium carboxymethyl cellulose (CMC; Sigma-Aldrich) with a molecular weight of 250 kg/mol. To prepare the composite, a CMC solution was prepared with 2 wt. % concentration in de-ionized water. Carbon black was then added to the CMC solution and dispersed using a rotor-state homogenizer. Finally, the graphite was added to the carbon black-CMC paste and mixed using an ARE-310 planetary centrifugal mixer. The prepared slurry had 33 wt. % of graphite, 1.3 wt. % of carbon black, and 1.3 wt. % of CMC. The rheological properties were measured with a cup-bob geometry with an inner diameter of 10 mm and a cone-plate geometry of diameter 50 mm and 1° angle at 20 °C.

The wormlike micelle (WLM) solution was composed of 3.58 wt. % of cetylpyridinium chloride (CPCl) purchased from Spectrum Laboratory in a de-ionized water solution of sodium salicylate (NaSal) purchased from Sigma-Aldrich with a molar ratio of NaSal to CPCl equal to 0.65. The solution was prepared by first adding the desired amount of NaSal to de-ionized water followed by adding CPCl. All the contents were then shaken inside a bottle and left for at least 2 days for equilibration before rheometric testing. The rheological properties were measured with a cone-plate geometry of diameter 50 mm and angle 2° at 23.5 °C.

The linear low-density polyethylene (LLDPE) was supplied from Hanwha Solutions (LLD3126). The molecular weight and softening point is 130 kg/mol and 103 °C, respectively. LLDPE samples were prepared as disk-shape pellets by a hot press. The pellet thickness was 1.2 mm, and the diameter was 8 mm. The rheological properties were measured with a plate-plate geometry of diameter 8 mm. The master curves were constructed with a reference temperature of 155 °C.

B. Rheometry

Rheological measurements were performed on an MCR-302 rheometer from Anton Paar and a DHR-3 rheometer from TA Instruments using various geometries at varying temperatures as mentioned in Sec. III A. Frequency sweep tests were carried out before and after each measurement and were compared to confirm that there was no critical issue in oxidation or degradation of PS at a high temperature and in water evaporation of solution systems.

C. Recovery rheology test

The main concept behind recovery rheology is that strain is a composite parameter consisting of two measurable components. To distinguish the recoverable and unrecoverable strains, constrained recovery tests, where the shear stress is set to zero and the material is allowed to recover, can be carried out following any protocol. For instance, oscillatory or steady shearing where the strain is controlled can be followed by an imposition of zero-shear stress and some portion of the total deformation can be seen to recover. The part that recovers is called the "recoverable strain", $\gamma_{rec}(t)$, and the remaining amount is called the "unrecoverable strain", $\gamma_{un}(t)$. By iterating this process of performing constrained recovery tests, time-resolved recoverable and unrecoverable strain can be obtained, $\gamma(t) = \gamma_{rec}(t) + \gamma_{un}(t)$. While the iterative recovery test provides material functions and time-resolved information, the average material functions can be obtained simply through the strain shift test detailed in Sec. III C 2.

1. Iterative recovery test

When performing iterative recovery tests for the start-up of shear, a zero-rate step was applied for a very short duration of time, 0.04 s, immediately after the shearing step and just before the recovery step. This was inserted to make sure that the rheometer geometry did not move further after the shearing step due to inertia. The duration of the quiescent step was sufficiently longer than the instrument response time of around 0.01 s, yet still short enough not to have any significant effect on the material process. Each measurement of recoverable strain is a separate test, which involves the application of deformation up to a certain instant, followed by a constrained recovery step where the applied shear stress is set to zero. This process is iteratively performed to build a time-resolved dataset, as shown in Fig. 2.

2. Strain shift test

In a stress-controlled oscillatory shear test, even if we impose a stress wave function that starts at 0, the strain response can end up oscillating about a nonzero value referred to as the strain shift, γ_s , as shown in Fig. 3. The strain shift is attributed to the acquisition of unrecoverable strain [52]. The measurable strain shift, therefore, allows us to calculate three moduli, G'_{solid} , G''_{solid} , and G''_{fluid} , derived from the recoverable and unrecoverable strains. The details regarding these calculations can be found in Lee *et al.* [52] and Griebler *et al.* [62]. In this section, we describe how to calculate G''_{fluid} and $G''_{fluid,raw}$ using the stress, strain amplitude, and the strain shift.

The strain shift experiments were performed on a TA Instruments DHR-3 torque-controlled rheometer using a parallel plate geometry with a 25 mm diameter at varying temperature. Since the TRIOS software reports any strain response data as oscillating about zero when using the built-in oscillatory functions, strain shift experiments must be performed under the "Arbitrary Wave" function in the TRIOS software. The stress wave function was applied as $\sigma_0 \sin(\omega t_{test} + \psi)$, where σ_0 is the stress amplitude, ω is the

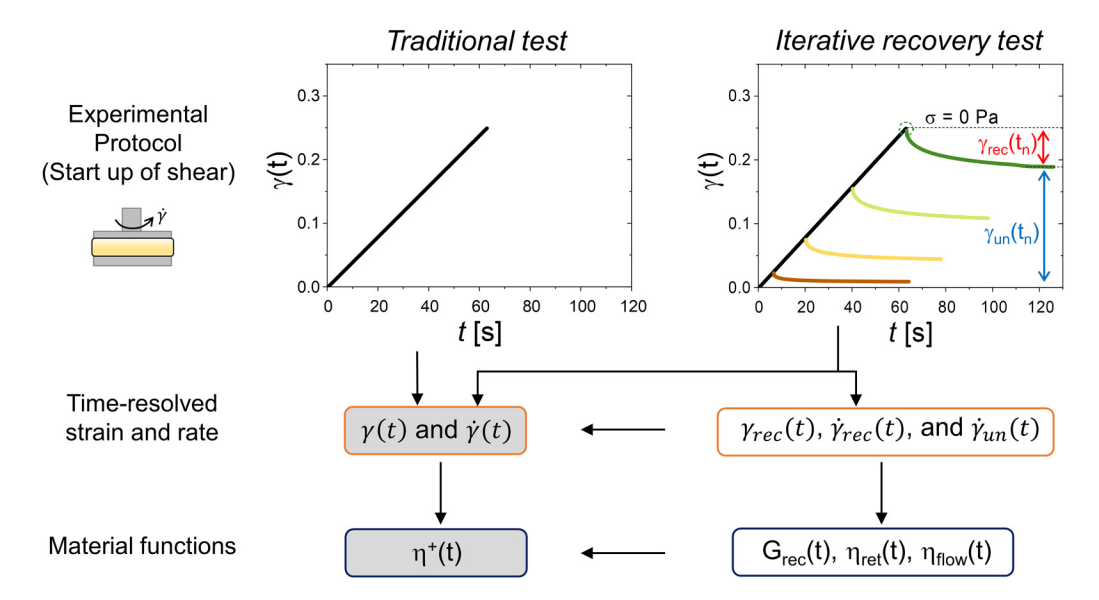


FIG. 2. Comparison between traditional rheology and recovery rheology in the start-up of the shear test. While the recovery rheology allows us to get modulus, G_{rec} , and two viscosities, η_{ret} and η_{flow} , in this study, we only use the flow viscosity, η_{flow} , considering that the Cox–Merz rule deals with the steady shear viscosity.

angular frequency, and ψ is the phase angle of the applied stress wave. For simplicity, $\psi = 0$ was selected so that sinusoidal stresses were applied to maximize the strain shift. Zero-stress steps were added before and after the stress wave function, each holding the shear stress at zero for twait and t_{recover} to compare all subsequent strain measurements with the original starting position. Thus, a series of stress wave functions for the strain shift test consists of (1) 0 Pa for t_{wait}, (2) $\sigma_0 \sin(\omega t_{test} + \psi)$ for t_{test} , and (3) 0 Pa for $t_{recover}$. While twait and trecover are determined as the time for the material to recover sufficiently to exhibit at least 95% of the total recoverable strain, the testing time, t_{test}, is set so that 10 periods are completed at a given angular frequency. A series of stress wave functions is repeated three times in the forward, $\sigma_0 > 0$, and reverse, $\sigma_0 < 0$, directions to account for possible instrument drift. Then, the resulting strain wave functions are obtained, $\gamma(t_{test}) = \gamma_s + \gamma_0 \sin(\omega t_{test} + \delta)$.

Using the parameters obtained from the strain shift test, the contribution to the fluid component of the loss modulus, G''_{fluid} , is calculated as

$$G_{fluid}^{"} = \frac{\sigma_0 \gamma_s}{\gamma_0^2 \cos(\psi)}.$$
 (18)

The total loss modulus, G'', can be easily obtained in the traditional oscillatory test, but it can be also calculated using the parameters in the strain shift test. The detailed equations to derive G''_{solid} , and G''_{fluid} are given in Appendix A.

Since G''_{fluid} indicates the dissipated energy normalized by the total strain amplitude, γ_0 , if we want to gain information from the material perspective, it is more natural to use the component moduli normalized with its respective component strain amplitude [57,62]. In this study, $G''_{fluid,raw}$ is used to

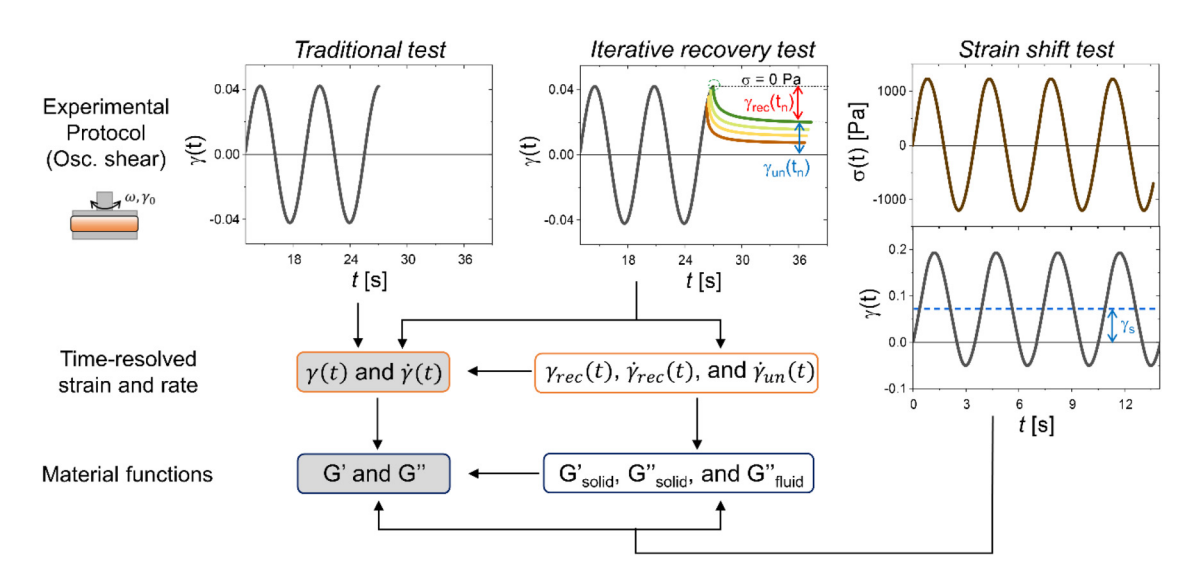


FIG. 3. Comparison between traditional rheology and recovery rheology in the oscillatory shear test. The three decomposed moduli $(G'_{solid}, G''_{solid}, \text{ and } G''_{fluid})$ can be obtained from both the iterative recovery test and the strain shift test.

interpret the material response as

$$G''_{fluid,raw} = \frac{\sigma_0}{\gamma_s \cos(\psi)} \ . \tag{19}$$

IV. RESULT AND DISCUSSION

In this work, we have focused our presentation on the PS of $\rm M_w$ = 192 000 g/mol at a reference temperature of 180 °C because PS was one of the original materials used in the first publication reporting the Cox–Merz rule [1]. While Cox and Merz reported only the results on polymer melts at high temperatures (200–232 °C) above the melting temperature of the polymer, we present the results at a wide range of temperatures and frequencies using time-temperature superposition. Additionally, to demonstrate that revisiting the empirical rules is not limited to a specific material, we include other examples including a surfactant system, a polymer hydrogel, a GO suspension, and a model battery slurry.

A. Traditional rheological characterization

We performed the start-up of shear tests at 180 °C by applying constant shear rates to the PS in the range of 0.01 to 2.51 s⁻¹. The stress growth function and the stress growth coefficient are presented in Figs. 4(a) and 4(b). At low shear rates where the flow is weak, the stress growth coefficient, $\eta^+(t)$, increases gradually up to the zero-shear viscosity, η_0 , without overshooting. At high shear rates, where the flow is strong, $\eta^+(t)$ exhibits an overshoot before reaching a plateau at the steady-shear viscosity $\eta_{ss} < \eta_0$. The tests terminate at the solid symbols shown in Figs. 4(a) and 4(b), which mark whichever is earlier: 600 s or the point where edge fracture initiates. The steady-shear viscosity, η_{ss} , is taken as the value of $\eta^+(t)$ at these points, and is shown as a function of the applied shear rate in Fig. 4(c) up to a rate of $2.51 \,\mathrm{s}^{-1}$. Application of rates higher than this result in rapid edge fracture of the sample before any steady state can be achieved, as shown in the inset of Fig. 4(c).

The linear viscoelastic behavior of entangled PS in the frequency range from 10^{-2} to 10^5 rad/s is shown in Fig. 5. The time temperature superposition (TTS) master curves, shown

as moduli and the magnitude of the complex viscosity, are constructed with a reference temperature of 180 °C. In Fig. 5(a), at low frequencies, a terminal region is observed with the usual scaling of $G' \sim \omega^2$ and $G'' \sim \omega$. The reptation time, τ_{rep} , and the Rouse time of an entanglement strand, τ_e , are determined by the intersection of the dynamic moduli [65].

We show in Fig. 5(b) how the magnitude of the complex viscosity is constant at the value of the zero-shear viscosity, η_0 , at low frequencies and starts to decrease above about 0.1 rad/s. The Cox-Merz rule is an equality between the magnitude of the complex viscosity and the steady shear viscosity when the frequency is numerically the same as the shear rate. To examine this equality, in Fig. 5(c), the magnitude of the complex viscosity and the dynamic viscosity are divided by the steady shear viscosity. At low frequencies, the complex viscosity and the dynamic viscosity are the same as the steady shear viscosity and Cox-Merz holds. However, with increasing frequencies and shear rates, the complex viscosity becomes significantly larger than the steady shear viscosity, indicating that the failure of the Cox-Merz rule is frequency and rate dependent. The magnitude of the complex viscosity consists of elastic and viscous moduli, G' and G'', while the dynamic viscosity is related only to G''. It is, therefore, expected that the dynamic viscosity ought to be a better approximation of the steady-shear viscosity, as is shown in Fig. 5(c). As described in Eq. (9), the dynamic viscosity, $\eta' = G''/\omega$, consists of recoverable and unrecoverable components. In Fig. 5(c), The dynamic viscosity, η' , also becomes significantly larger than the steady shear viscosity as the frequency increases. This implies that the failure of the Cox-Merz rule lies in the composite nature of the dynamic $\frac{80}{60}$ viscosity rather than simply the elastic component of the material. Further details will be discussed in Secs. IV B and IV C.

B. Start-up of shear test and oscillatory shear test with recovery rheology

In Fig. 6, we show a representative result of the start-up of shear test using recovery rheology metrics at a shear rate of 0.251 s⁻¹. Since we impose a constant total shear rate, the total strain increases linearly. However, through the iterative

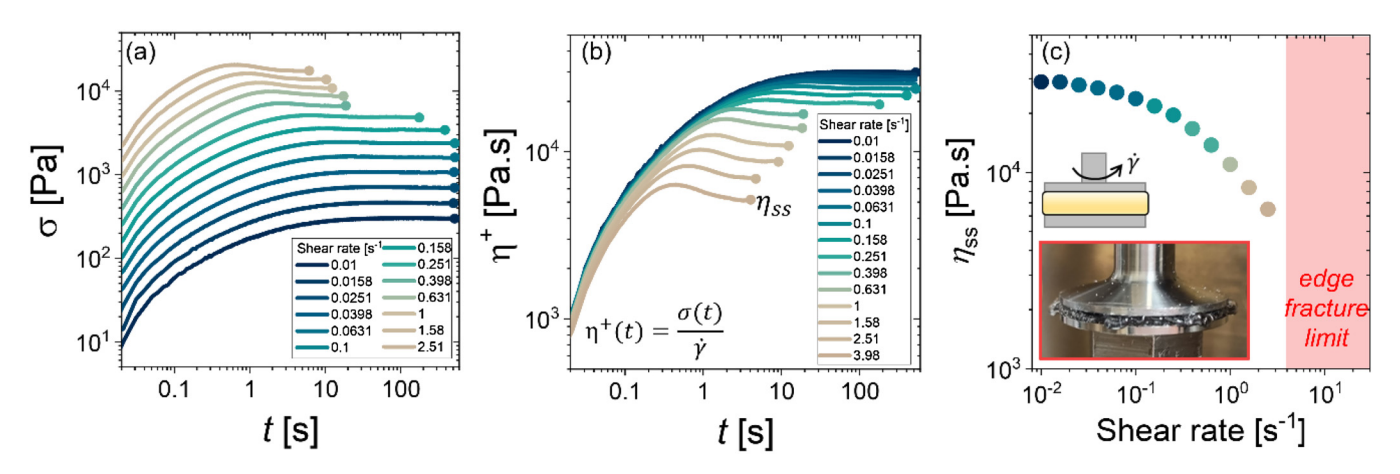


FIG. 4. Start-up of the shear test with traditional rheology at 180 °C. At given shear rates, (a) total stress and (b) the stress growth coefficient, η^+ , over time. (c) Steady-shear viscosity, η_{ss} , obtained from the plateau of (b). The inset of (c) shows the photo when the sample results in edge fracture at high shear rates.

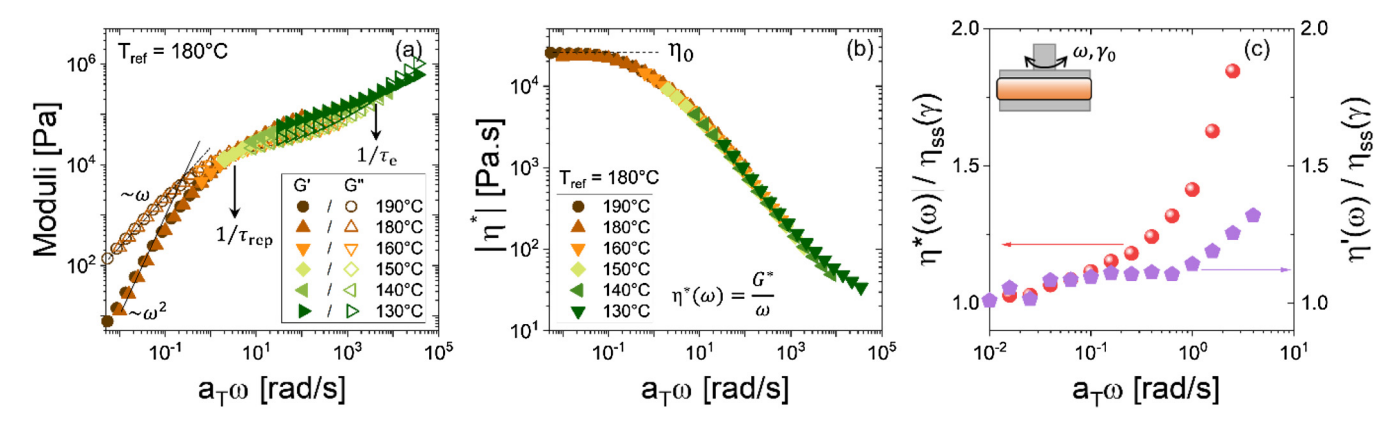


FIG. 5. Frequency sweep with traditional rheology. The master curves of (a) moduli and (b) complex viscosity for PS-192k constructed at a reference temperature of 180 °C. The temperature range is from 130 to 190 °C. Two relaxation times are presented τ_{rep} is the reputation time and τ_e is the Rouse time of an entangled strand. Horizontal shift factors, a_T , of TTS from PS-192k are in Appendix B. (c) The ratio of the complex viscosity and the steady shear viscosity and the ratio of dynamic viscosity and the steady shear viscosity as a function of angular frequency. The steady shear viscosity in Fig. 4(c) is used.

recovery tests, the strain can be decomposed into recoverable and unrecoverable strains, which do not increase linearly in time, as shown in Fig. 6(b). Therefore, the imposed total strain rate is constant but the recoverable and unrecoverable strain rates are not always, as observed in Fig. 6(c). In the initial stages, the recoverable strain rate is equal to the imposed shear rate while the unrecoverable strain is initially zero. That is, recovery rheology shows that all strain is

initially acquired recoverably. Over time, the recoverable strain rate decreases to 0 and the unrecoverable strain rate increases to the imposed shear rate. The steady-shear viscosity, therefore, reflects the purely unrecoverable response at zero recoverable strain rate as shown in Fig. 6(c),

$$\eta_{ss}(\dot{\gamma}) = \frac{\sigma_{ss}}{\dot{\gamma}} = \frac{\sigma_{ss}}{\dot{\gamma}_{un}} \ . \tag{20}$$

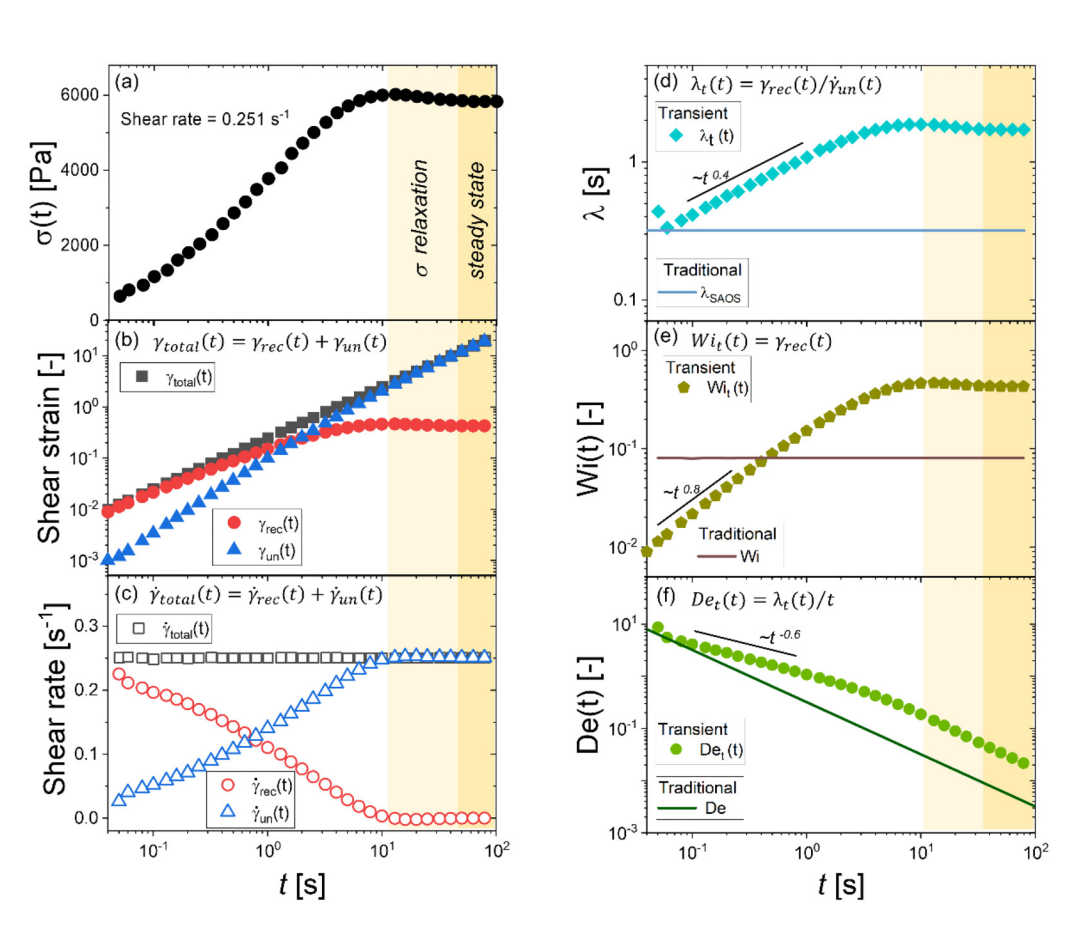


FIG. 6. Start-up of the shear test with recovery rheology at $180\,^{\circ}$ C. (a) Total stress, (b) the decomposed total strain into the recoverable and unrecoverable strains, and (c) their corresponding rates of acquisition for an applied shear rate of $0.251\,\mathrm{s}^{-1}$. Each data point was collected using the iterative recovery test. (d)–(f) The relaxation time and dimensionless groups defined with traditional rheology are presented by the lines, while those newly defined using recovery rheology are presented by the symbols. (d) The relaxation time, (e) the Weissenberg number, and (f) the Deborah number during start-up of shear.

Moreover, the transition of the material acquiring strain recoverably to unrecoverably can be interpreted as a transition in response from that of a viscoelastic solid to a viscous fluid. This transition implies that flow strength from the material perspective is not consistent during the test.

To characterize the flow strength, we turn to the use of dimensionless groups. Two particular groups that quantify dimensionless flow strength and a timescale of deformation are the Weissenberg number and the Deborah number, which represent the ordinate and abscissa of "Pipkin space" to describe the material deformations in a universal way [66].

The Weissenberg number, typically denoted as Wi, was first proposed by White [67] to describe the strength of the flow. He described the Weissenberg number as being seen to represent the amount of recoverable strain in the fluid. A typical modern writing of the Weissenberg number is given as $\lambda \dot{\gamma}$, where λ is the relaxation time and $\dot{\gamma}$ is the applied shear rate. The relaxation time today is usually taken to be the longest relaxation time from the SAOS measurement. In this case, the relaxation time is usually considered a constant value in any shear protocol, so the Weissenberg number is often interpreted as dependent only on the shear rate.

The Deborah number, typically denoted as De, was first introduced by Reiner [68] to describe how solidlike or liquidlike a material behaves. He suggested the Deborah number as the ratio of the material relaxation time (λ) to the experimental observation time (t_{obs}). Therefore, when the relaxation time is constant, the Deborah number is proportional to the reciprocal of the experiment time and is considered a dimensionless number unrelated to the shear rate.

The traditional relaxation time and two dimensionless numbers at a fixed shear rate of $0.251 \,\mathrm{s}^{-1}$ are shown as solid lines in Figs. 6(d)–6(f). While the traditional relaxation time and the Weissenberg number exhibit constant values at all times due to the fixed shear rate and the assumption of an unchanging relaxation time, the traditional Deborah number deceases as the reciprocal of time. The traditional approach that determines the relaxation time from SAOS measurement (λ_{SAOS}) makes an implicit assumption that the relaxation time of the material is consistent under any shear protocol, even in the nonlinear regime. In fact, the relaxation time can depend on the flow strength, so using λ_{SAOS} to represent relaxation processes at all times can lead to ambiguity in interpreting the time-resolved nonlinear behavior.

To avoid this ambiguity, we return to White's original presentation of the Weissenberg number [67]. He defined the Weissenberg number as

$$Wi = J_e \omega_1 U/L, \tag{21}$$

where J_e is the steady-state recoverable shear compliance, $J_e = \gamma_{rec}/\sigma$, ω_1 is White's symbol for the viscosity defined as $\omega_1 = \eta = \sigma/\dot{\gamma}$ [60,66], and U/L is the shear rate $\dot{\gamma}$, so that

$$J_e \omega_1 U/L = \frac{\gamma_{rec}}{\sigma} \frac{\sigma}{\dot{\gamma}} \dot{\gamma} = \gamma_{rec}, \tag{22}$$

making clear his suggestion of the Weissenberg number as the amount of recoverable strain in the fluid. If we take the common modern interpretation of the Weissenberg number as the product of the relaxation time and the shear rate, $Wi = \lambda \dot{\gamma}$, then,

$$\lambda = J_e \omega_1 = \frac{\gamma_{rec}}{\dot{\gamma}_{un}}.$$
 (23)

Therefore, the Deborah number can be (re)defined as

$$De = \frac{\lambda}{t_{obs}} = \frac{\gamma_{rec}}{\dot{\gamma}_{un}} \frac{1}{t_{obs}} . \tag{24}$$

Once we acknowledge the recoverable and unrecoverable components as being measurably separate from the total strain, the relaxation time and dimensionless groups can be (re)defined as time-resolved parameters reflecting the nonlinear behavior as presented in Eqs. (22)-(24). These timeresolved parameters at a shear rate of 0.251 s⁻¹ are presented in Figs. 6(d)-6(f) as $\lambda_t(t) = \gamma_{rec}(t)/\dot{\gamma}_{un}(t)$, $Wi_t(t) = \gamma_{rec}(t)$, and $De_t(t) = \lambda_t(t)/t$. Additionally, the Deborah number can be simplified as the ratio of recoverable rate and unrecoverable rate, $\dot{\gamma}_{rec}/\dot{\gamma}_{un}$, as reported in the study of Singh et al. [63]. While λ_{SAOS} is independent of the observation time and is always equal to $1/\tau_{rep}$, $\lambda_t(t)$ initially increases with a scale of $t^{0.4}$ and levels off at a steady state. Similarly, $Wi_t(t)$ is also initially time-dependent with a scale of $t^{0.8}$ before eventually saturating at a steady state, whereas the traditional N Weissenberg number is independent of the time scale.

The traditional and time-resolved Deborah numbers start of the same values, but their subsequent trends are significantly different. At early times, when the recoverable response is dominant, $De_t(t)$ decreases with a scale of $t^{-0.6}$, implying that the material yields more slowly than traditionally expected. When the unrecoverable response becomes dominant and reaches a steady state, $De_t(t)$ finally decreases with a scale of t^{-1} and gets close to zero [69], suggesting the fluidization of the material.

The decomposed strain also allows us to obtain the time-resolved flow viscosity, $\eta_{flow}(t)$, by dividing the stress by the unrecoverable strain rate as described in Eq. (12). In Fig. 7(a), the flow viscosity is compared with the stress growth coefficient. The difference between their definitions is the denominator: $\eta_{flow}(t) = \sigma(t)/\dot{\gamma}_{un}(t)$ and $\eta^+(t) = \sigma(t)/\dot{\gamma}_{total}(t)$. The two metrics are, therefore, different by a factor of $\dot{\gamma}_{total}(t)/\dot{\gamma}_{un}(t)$. Given that the total rate is composite and is made of recoverable and unrecoverable parts, this ratio can be written as $\dot{\gamma}_{total}(t)/\dot{\gamma}_{un}(t) = (\dot{\gamma}_{rec}(t) + \dot{\gamma}_{un}(t))/\dot{\gamma}_{un}(t) = 1 + \dot{\gamma}_{rec}(t)/\dot{\gamma}_{un}(t)$, which, under conditions stated above, could be seen as 1 + De. That is, when elasticity plays a significant role, making De > 1, the flow viscosity and stress growth coefficient will be significantly different.

Despite being a shear thinning material, as shown in Fig. 4(c), as the imposed shear rate increases, the flow viscosity, $\eta_{flow}(t)$, always starts from the zero-shear viscosity, η_0 , as shown in Fig. 7(b). This behavior is consistent with the study of Singh *et al.* [63] that revisited the definitions of transient rheological material functions. Therefore, the transient stress signal is encompassed by the components of the strain, rather

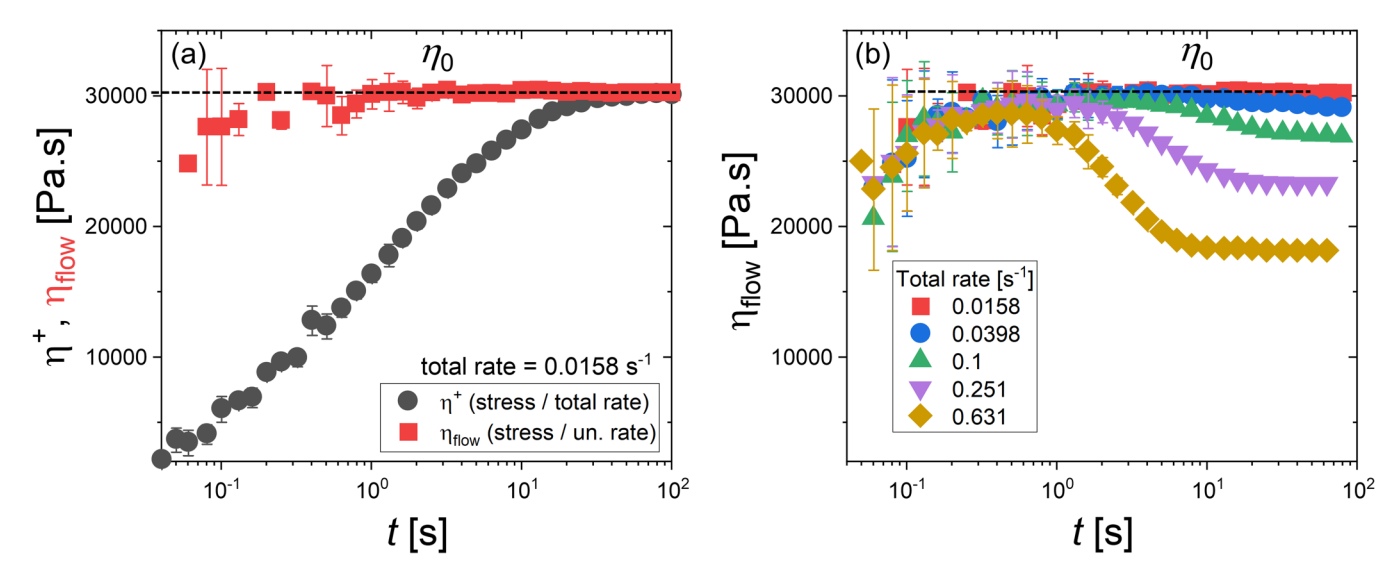


FIG. 7. (a) Comparison between the stress growth coefficient, η^+ , and the time-resolved flow viscosity, $\eta_{flow}(t)$, defined as the ratio of stress and unrecoverable strain rate. (b) The time-resolved flow viscosity at varying shear rates. At all shear rates, the flow viscosity starts from zero-shear viscosity, η_0 .

than the material functions such as the stress growth coefficient. This implies that the decomposed strain allows for a clearer interpretation of the rheological phenomenon.

C. Revisiting the Cox-Merz rule

As discussed in Sec. II.A, the complex viscosity is a composite parameter consisting of recoverable and unrecoverable responses, while the steady shear viscosity comes just from unrecoverable deformation. The composite nature of the complex viscosity may, therefore, be at the heart of the failure of the Cox–Merz rule. Since η' is consists of recoverable and unrecoverable components, a fairer comparison is between the unrecoverable component of η' and the steady shear viscosity.

Recovery rheology decomposes the loss modulus into solid and fluid components, G''_{solid} , and G''_{fluid} . The subscripts "solid" and "fluid" represent the material functions attributed to the recoverable and unrecoverable strains.

We show in Fig. 8(a) the recoverable and unrecoverable components of the loss modulus, G''_{solid} and G''_{fluid} . In the terminal region, where G'' > G', G'' is made up of mostly the unrecoverable strain contribution, $G''_{fluid} > G''_{solid}$. In contrast, in the rubbery region, where G' > G'', G''_{solid} becomes larger than G''_{fluid} , indicating that energy dissipation from the acquisition of recoverable strain contributes significantly to the material behavior.

A useful measure for whether Cox-Merz might be $\frac{8}{2}$ expected to apply is therefore the ratio η'_{solid}/η' , which is the same as the ratio G''_{solid}/G'' . As shown in Fig. 8(b), the contribution of G''_{solid} becomes an increasingly larger fraction of the total energy dissipated with increasing frequencies. By the relations between dynamic moduli and viscosities, this suggests that the dynamic viscosity, η' , results predominantly from the contribution of the unrecoverable strain at low frequencies, but from the recoverable strain at high frequencies.

The composite nature of the dynamic loss modulus and dynamic viscosity implies that the complex viscosity obtained from the traditional G'' is also a composite

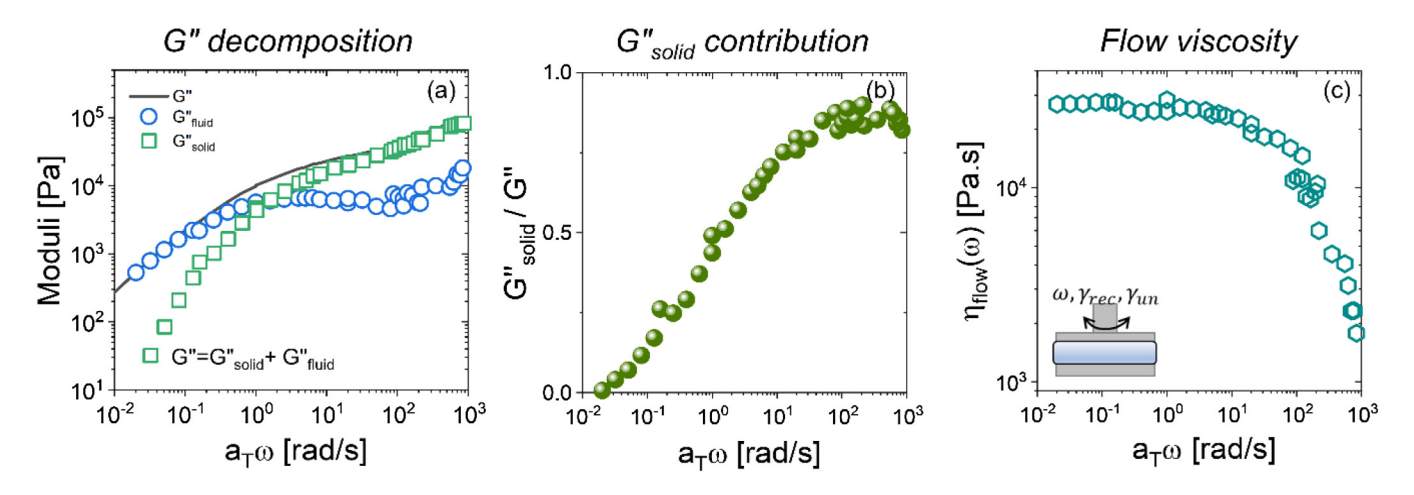


FIG. 8. Frequency sweep with recovery rheology at a reference temperature of 180 °C. (a) The decomposed moduli. The solid line indicates G" that can be decomposed into the solid and fluid component of loss modulus. (b) The solid component of loss modulus divided by traditional loss modulus. The increase in this value indicates that recoverable response becomes dominant at a given frequency. (c) Flow viscosity as shown in Eq. (14).

parameter that includes both recoverable and unrecoverable deformation of the material. Since $G_{solid}^{\prime\prime}$ and $G_{fluid}^{\prime\prime}$ are the dissipated energy rates normalized by the total strain amplitude, they are suitable for quantitative comparisons of whether recoverable or unrecoverable deformation is dominant. However, considering that recovery rheology takes the perspective that strain is separable, it is more effective to normalize the component moduli by their respective component strain amplitudes, such as in $G''_{fluid,raw}$, which represents the unrecoverable deformation of the material as shown in Eqs. (13) and (14). Since $G''_{fluid,raw}$ is the material function obtained from the unrecoverable components, using $G''_{fluid,raw}$ gives the flow viscosity, η_{flow} , rather than the complex viscosity during the oscillatory shear test. In Fig. 8(c), the flow viscosity of the PS is presented as $G''_{fluid,raw}$ divided by the frequency, $\eta_{flow} = G''_{fluid,raw}/\omega$.

The steady-shear viscosity, η_{ss} , reflects the response of a material to acquisition of purely unrecoverable strain, while the dynamic viscosity, η' , is a composite parameter that contains both recoverable and unrecoverable contributions. The magnitude of the complex viscosity cannot, therefore, always correspond to steady shear viscosity. In Fig. 9(a), we show that the magnitude of the complex viscosity and the steady-shear viscosity of the PS gradually deviate more as the frequency increases due to the larger contribution of the recoverable components as discussed above and shown in Fig. 8.

The difference between the magnitude of the complex viscosity and the steady-shear viscosity, as seen in Eqs. (15) and (20), is the denominator. The complex viscosity is defined by the total rate, while the steady-shear viscosity is defined by the unrecoverable rate. The two metrics are therefore different by a factor of the total strain rate over unrecoverable strain rate. If we expand the total rate as the sum of recoverable and unrecoverable strain rate, the factor simplifies to being less than or equal to $\dot{\gamma}_{rec}/\dot{\gamma}_{un}+1$. Since the ratio of rate components can represent the Deborah number as discussed earlier, the factor can be simplified as De+1. This means that the deviation between the magnitude of the complex viscosity and the steady-shear viscosity depends on De+1. At low De, more strain is acquired unrecoverably

while at high *De*, more strain is acquired recoverably. Thus, the Cox–Merz rule fails in the regime where the recoverable response becomes dominant.

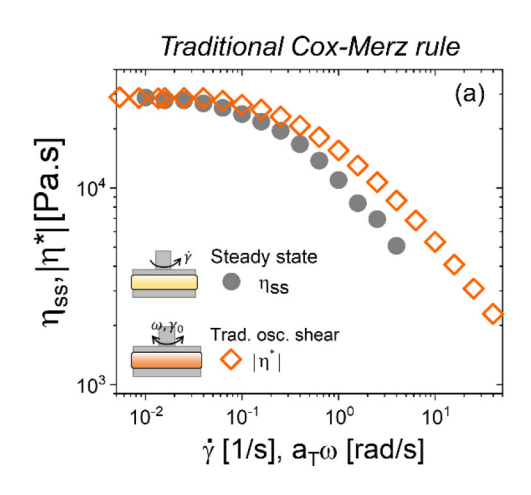
We show in Fig. 9(b) the viscosity comparison for the steady shear viscosity, η_{ss} , and the flow viscosity obtained from oscillatory shearing, $\eta_{flow} = G''_{fluid,raw}/\omega$, of the PS melt. Both parameters are attributed to acquisition of unrecoverable strain; thus, the steady shear viscosity is superposed to the flow viscosity without limitation of the frequency or shear rate.

This relation is not limited to the specific polymer melt we show in Fig. 9, but rather works for various systems. We show in Fig. 10 the results for a hydrogel, an anode battery slurry, anisotropic GO colloids, a self-assembled micelle system, and branched polymers. The insets in each panel represent the traditional Cox-Merz measures and the results of the frequency sweep for each material are in Appendix C. Among the materials, a self-assembled micelle system in Fig. 10(d) is one of the typical Maxwell fluid model systems with only unrecoverable dissipated energy. The Cox-Merz rule works for the material that either has no recoverable G" or has a large contribution of unrecoverable dissipated energy. In contrast, the agreement between the unrecoverable metrics across all materials we have studied suggests a universality. Even when applied to a material that exhibits shear-thickening behavior, shown in Fig. 10(a), in which the Cox-Merz rule fails, the unrecoverable viscosity comparison still works successfully.

The general formalism of the unrecoverable viscosity somparison can be described as

$$\eta_{ss}(\dot{\gamma}) = \eta_{flow}(\omega)|_{\omega\gamma_{un} = \dot{\gamma}},$$
(25)

where γ_{un} is the unrecoverable strain, which can be replaced with strain shift, γ_s . While the traditional Cox–Merz rule is limited in the SAOS regime and the Rutgers–Delaware rule is limited in the large amplitude oscillatory shear (LAOS) regime, the unrecoverable viscosity comparison in Eq. (25) works in both SAOS and LAOS regimes. To predict the steady-shear viscosity at high shear rates, there are two approaches in oscillatory sweeps: increasing frequency or



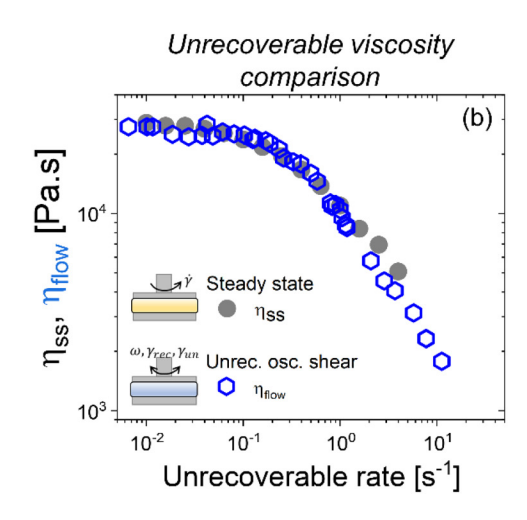


FIG. 9. (a) Comparison between the steady-shear viscosity and the magnitude of the complex viscosity by accepting the traditional Cox–Merz rule of the PS melt at a reference temperature of 180 °C. At high frequencies, the Cox–Merz rule fails showing that the magnitude of the complex viscosity becomes larger than the steady-shear viscosity. (b) New relations between the steady-shear viscosity and the flow viscosity, η_{flow} , obtained from unrecoverable strain.

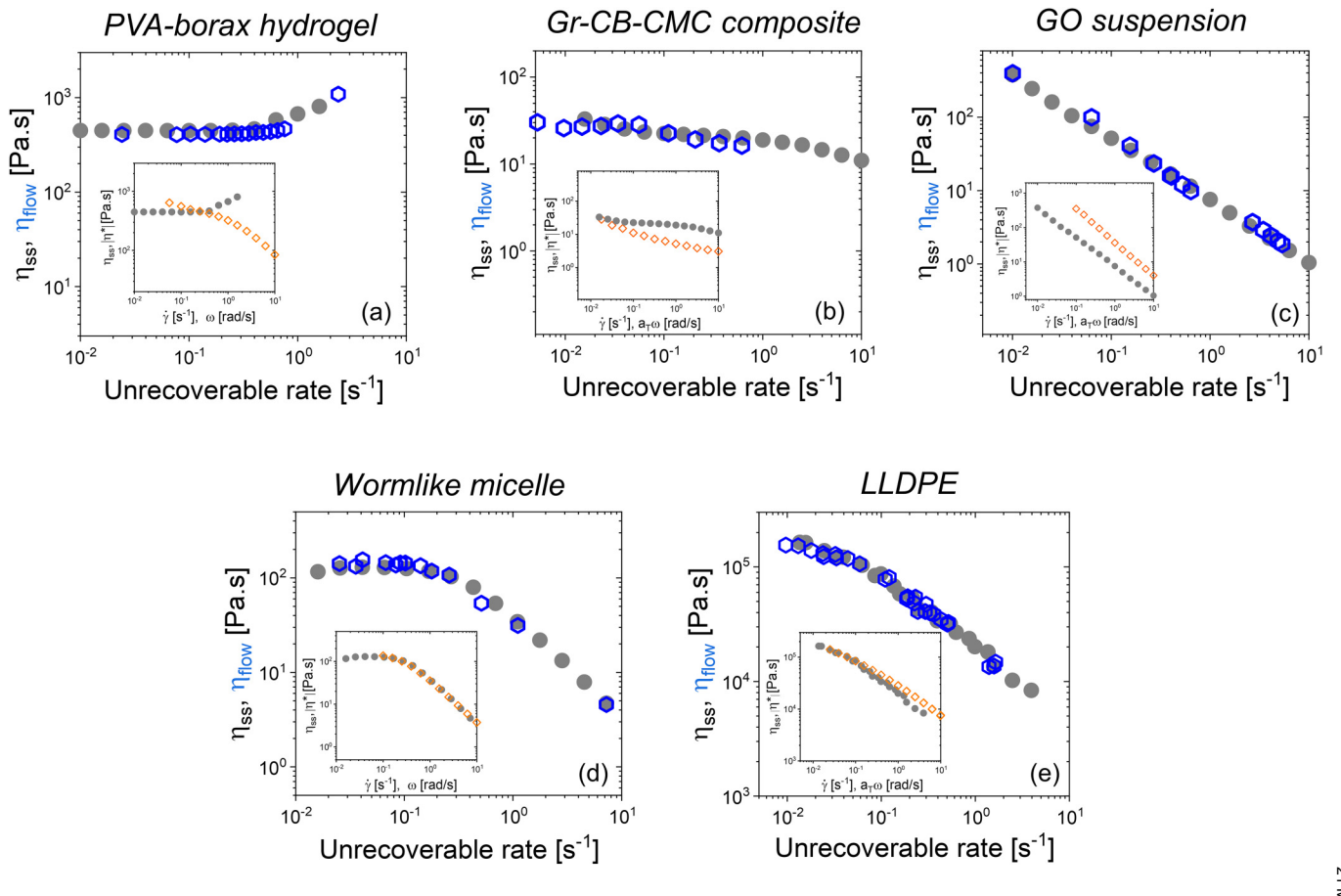


FIG. 10. Unrecoverable viscosity comparison of (a) PVA-borax hydrogel, (b) graphite-carbon black-CMC polymer composite as an anode slurry system, (c) of Suspension, (d) WLM systems, and (e) LLDPE as a branched polymer system. Each material represents shear-thickening material, anode battery slurry, anisotropic colloid, and surfactant system, respectively. The circle and hexagonal symbols indicate the steady-shear viscosity and the unrecoverable flow viscosity, respectively. The inset of each figure is the result of the traditional Cox-Merz rule by comparing the steady-shear viscosity and the magnitude of the complex viscosity. The diamond symbol indicates the magnitude of the complex viscosity. The results of frequency sweep are presented in Appendix C.

amplitude. Figures 10(a)–10(d) show the flow viscosity with increasing amplitude at a fixed frequency, including SAOS and LAOS regimes. In contrast, Figs. 9 and 10(e) show the flow viscosity with varying frequencies in the SAOS regime. The flow viscosity is all superposed on the steady-shear viscosity, suggesting a universality of the unrecoverable viscosity comparison.

Using recovery rheology, therefore, allows us to predict the steady-shear viscosity from oscillatory shear testing by extracting the unrecoverable information as described in Eq. (25). We only need one additional piece of information to decompose the parameter into recoverable and unrecoverable parts. The strain shift test provides this extra information while simultaneously unrecoverable flow viscosity as laid out in Eqs. (16) and (17) keeps the benefits of the Cox–Merz rule while overcoming the assumption that all strain is acquired unrecoverably in oscillatory tests. It may, therefore, be possible to predict the steady-shear viscosity from SAOS and even LAOS data of all materials while avoiding the issues of sample instability from the nonlinear properties in the steady shear response.

V. SUMMARY AND CONCLUSION

In this study, we investigated the rheological physics behind the empirical Cox-Merz rule using recovery rheology. While this empirical rule is based on the total strain, recovery rheology highlights the difference between the steady-shear and complex viscosities. Recovery rheology, therefore, provides parameters that allow us to clearly interpret the material response across protocols. Our reexamination of the empirical Cox–Merz rule through the lens of recovery rheology can be summarized by three major points,

- 1. A clear understanding of material functions. The Cox-Merz rule compares the steady shear viscosity, $\eta_{ss}(\dot{\gamma})$, and magnitude of the complex viscosity, $|\eta^*(\omega)|$. Recovery rheology thinking makes it clear that the steady shear viscosity represents a purely unrecoverable response while the complex viscosity contains contributions from both recoverable and unrecoverable strains.
- 2. Why the empirical Cox-Merz rule fails or works. The complex viscosity is a composite parameter consisting of both recoverable and unrecoverable responses. The failure of the Cox-Merz rule depends on the contribution of recoverable response to the dissipated energy, G". If the dissipated energy acquired from the recoverable component is dominant over that from the unrecoverable response, the traditional Cox-Merz rule fails.
- Predicting steady-shear viscosity in a universal way. The steady-shear viscosity reflects a purely unrecoverable response. It can be predicted from oscillatory

shearing through the unrecoverable flow viscosity, $\eta_{ss}(\dot{\gamma}) = \eta_{flow}(\omega)|_{\omega\gamma_{um}=\dot{\gamma}}$, rather than the magnitude of the complex viscosity. As shown in Figs. 9 and 10, a relation between the steady shear viscosity and the unrecoverable flow viscosity may be universal.

Our results also explain why the Rutgers-Delaware rule works. When subjected to large amplitude oscillatory shearing of sufficient amplitude, yield stress fluids acquire strain nearly purely unrecoverably. The steady shear flow curve similarly reflects unrecoverable acquisition of strain, and so in the yielded region the magnitude of the complex viscosity is dominated by the same unrecoverable components that are probed in the steady shear tests.

Traditional empirical rules often fail, but when they work, their use has significant advantages. By viewing the Cox-Merz rule through the lens of recovery rheology, the conditions under which it works and fails have been shown, and a new relation has been proposed that may be universal. As was the purpose of the traditional Cox-Merz rule, it is still possible to bridge two material functions obtained from different shear protocols. As long as material functions that come from the same strain components are used, the steady shear viscosity can be predicted from SAOS testing. This study, therefore, emphasizes the significance of recovery rheology, which provides more information than traditional testing alone, by decomposing the strain into recoverable and unrecoverable components. The extra information allows us to understand the connection between different metrics and provides a straightforward way to elucidate the rheological physics behind empirical rules.

ACKNOWLEDGMENT

This material was based upon work supported by NSF Grant No. 1847389.

AUTHOR DECLARATIONS

Conflict of Interest

The authors have no conflicts to disclose.

DATA AVAILABILITY

The data that support the findings of this study are available from the corresponding author upon reasonable request.

APPENDIX A: MODULI CALCULATION IN THE STRAIN SHIFT TEST

To calculate G''_{solid} and G''_{flulid} , we begin by examining storage and loss compliance in terms of energy dissipation and storage,

$$J'(\omega) = \frac{4(W_{stored}(\omega))_{avg}}{\sigma_0^2} = \frac{2[\sigma(t)\gamma(t)]_{avg}}{\sigma_0^2}, \quad (A1)$$

$$J''(\omega) = \frac{2(\dot{W}_{diss}(\omega))_{avg}}{\sigma_0^2 \omega} = \frac{2[\sigma(t)\dot{\gamma}(t)]_{avg}}{\omega \sigma_0^2}.$$
 (A2)

By acknowledging recoverable and unrecoverable strain rates, the loss compliance can be decomposed into solidlike and fluidlike components, as derived by Griebler *et al.* [62],

$$J_{solid}''(\omega) = \frac{2(\dot{W}_{diss,solid}(\omega))_{avg}}{\sigma_0^2 \omega} = \frac{2[\sigma(t)\dot{\gamma}_{rec}(t)]_{avg}}{\omega \sigma_0^2}, \quad (A3)$$

$$J''_{fluid}(\omega) = \frac{2(\dot{W}_{diss,fluid}(\omega))_{avg}}{\sigma_0^2 \omega} = \frac{2[\sigma(t)\dot{\gamma}_{un}(t)]_{avg}}{\omega \sigma_0^2}.$$
 (A4)

This can now be applied directly to the case of our experimental strain shift procedure. There is an equivalence in the concepts addressed by Eq. (A4), which represents the portion of the loss compliance that comes from unrecoverable dissipation of energy, and the strain shift, which also only comes from unrecoverable dissipation of energy. To develop a formal expression that links the two measures, we begin with the form $\sigma(t) = \eta \dot{\gamma}_{un}(t)$ for the unrecoverable strain rate and our sinusoidal stress to calculate the fluid component of the loss compliance from Eq. (A4). Since the average of any squared sine wave for an integer number of periods is equal to $\frac{1}{2}$, we see

$$J_{fluid}''(\omega) = \frac{2}{\omega \sigma_0^2} \left(\frac{\sigma_0^2 \sin^2(\omega t + \psi)}{\eta_{flow}} \right)_{avg} = (\omega \eta_{flow})^{-1}. \quad (A5)$$

We see from Eq. (A5) that the fluid component of the loss compliance is equal to the inverse of the angular frequency times the flow viscosity. This flow viscosity can be expressed in terms of the strain shift as follows:

$$\gamma_s = \frac{\sigma_0}{\omega \eta_{flow}} \cos \psi = \frac{\sigma_0}{\underline{\omega \sigma_0}} \cos \psi = \gamma_0 \cos \psi. \tag{A6}$$

Inserting Eq. (A6) into Eq. (A5), fluidlike loss compliance can be simplified as

$$J_{fluid}''(\omega) = \frac{\gamma_s}{\sigma_0 \cos \psi} . \tag{A7}$$

A similar process can be followed to calculate the connection between the flow viscosity and the fluid component of the loss modulus. In this case, G''_{fluid} can be described as

$$G''_{fluid}(\omega) = \frac{2}{\omega \gamma_0^2} \left(\frac{\sigma_0^2 \sin^2(\omega t + \psi)}{\eta_{flow}} \right)_{avg} = \frac{\sigma_0^2}{\gamma_0^2} (\omega \eta_{flow})^{-1} \quad (A8)$$

and the connection between the fluid component of the loss modulus and strain shift as follows:

$$G''_{fluid}(\omega) = \frac{\sigma_0 \gamma_s}{\gamma_0^2 \cos \psi} . \tag{A9}$$

We, therefore, have the link we sought between the strain shift measure, γ_s , and the fluid component of the loss modulus, G''_{fluid} . The solid component of the loss modulus follows directly from the additive nature of the loss modulus components shown in Eq. (9) by subtracting the fluid

component from the total,

$$G''_{solid} = G'' - G''_{fluid}. \tag{A10}$$

The fluid component moduli normalized with its respective component strain amplitude (i.e., $G''_{fluid,raw}$) can be obtained from Eq. (A6). Greibler *et al.* [57,62] reported that the flow viscosity corresponds to the ratio of $G''_{fluid,raw}$ and angular frequency as

$$\eta_{flow} = G''_{fluid,raw}/\omega.$$
(A11)

Inserting Eq. (A11) into Eq. (A6), $G''_{fluid,raw}$ is simplified as

$$G''_{fluid,raw} = \eta_{flow}\omega = \frac{\sigma_0}{\gamma_s \cos(\psi)}$$
 (A12)

These equations make it clear that if you apply a sinusoidal stress to any material and obtain the raw strain response including the strain shift, it is possible to distinguish between the components of the dynamic loss modulus without any extra experimentation.

APPENDIX B: SHIFT FACTOR OF PS-192 K

Figure 11 contains horizontal shift factors (a_T) of TTS from PS-192 k at $T_{\rm ref}$ = 180 °C. To construct the master curve in this work, we use a_T as a function of measurement temperature in Fig. 11. The temperature-dependence of the corresponding a_T is well fitted by the Williams–Landel–Ferry (WLF) model

$$\log(a_T) = \frac{-C_1(T - T_{ref})}{C_2 + T - T_{ref}}.$$
 (B1)

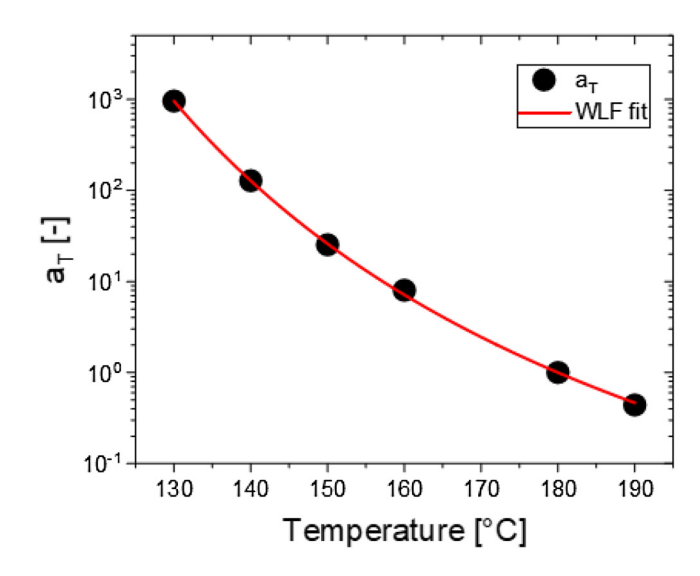


FIG. 11. Horizontal shift factors (a_T) of TTS from PS-192 k at $T_{ref} = 180$ °C.

The WLF model is used to fit the data and is shown as a dashed line. The WLF parameters are $C_1 = 4.5$ and $C_2 = 125.5$ K.

APPENDIX C: FREQUENCY SWEEP TEST

Figure 12 contains the results of the frequency sweep test for a hydrogel, an anode battery slurry, anisotropic GO colloids, a self-assembled micelle system, and branched polymers.

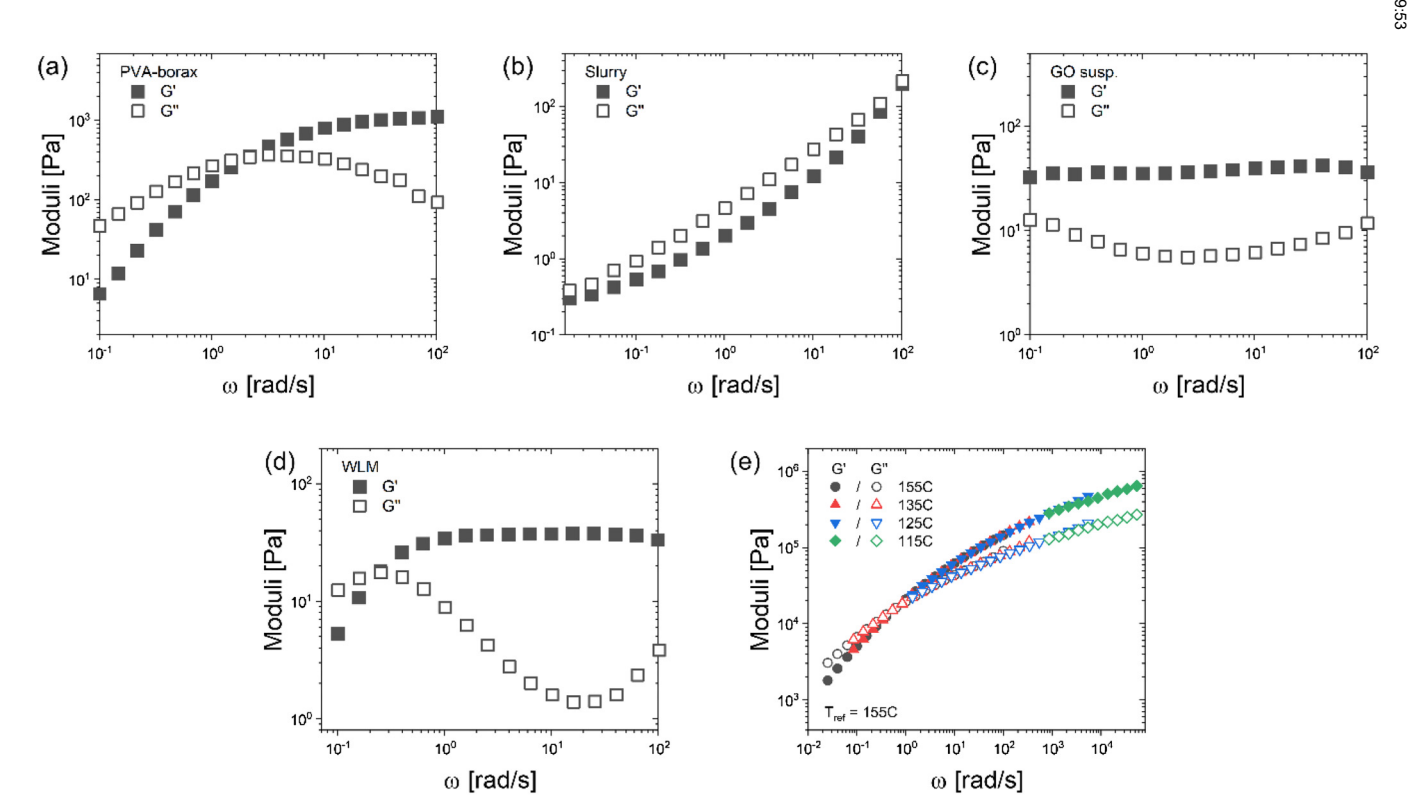


FIG. 12. Frequency sweep for (a) PVA-borax hydrogel, (b) graphite-carbon black-CMC polymer composite as an anode slurry system, (c) GO suspension, (d) WLM systems, and (e) LLDPE as a branched polymer system.

REFERENCES

- Cox, W., and E. Merz, "Correlation of dynamic and steady flow viscosities," J. Polym. Sci. 28, 619–622 (1958).
- [2] Winter, H. H., "Three views of viscoelasticity for Cox-Merz materials," Rheol. Acta 48, 241–243 (2009).
- [3] Sharma, V., and G. H. McKinley, "An intriguing empirical rule for computing the first normal stress difference from steady shear viscosity data for concentrated polymer solutions and melts," Rheol. Acta 51, 487–495 (2012).
- [4] Kulicke, W.-M., and R. Porter, "Relation between steady shear flow and dynamic rheology," Rheol. Acta 19, 601–605 (1980).
- [5] Laun, H., "Prediction of elastic strains of polymer melts in shear and elongation," J. Rheol. 30, 459–501 (1986).
- [6] Mansfied, C. D., T. Chen, M. Q. Ansari, and D. G. Baird, "The rheology of ultra-high molecular weight poly (ethylene oxide) dispersed in a low molecular weight carrier," Phys. Fluids 34, 023304 (2022).
- [7] Robertson, C. G., C. Roland, and J. Puskas, "Nonlinear rheology of hyperbranched polyisobutylene," J. Rheol. 46, 307–320 (2002).
- [8] Al-Hadithi, T., H. Barnes, and K. Walters, "The relationship between the linear (oscillatory) and nonlinear (steady-state) flow properties of a series of polymer and colloidal systems," Colloid Polym. Sci. 270, 40–46 (1992).
- [9] Yasuda, K., R. Armstrong, and R. Cohen, "Shear flow properties of concentrated solutions of linear and star branched polystyrenes," Rheol. Acta 20, 163–178 (1981).
- [10] Robertson, C., S. Warren, D. Plazek, and C. Roland, "Reentanglement kinetics in sheared polybutadiene solutions," Macromolecules 37, 10018–10022 (2004).
- [11] Chen, D., K. Molnar, H. Kim, C. A. Helfer, G. Kaszas, J. E. Puskas, J. A. Kornfield, and G. B. McKenna, "Linear viscoelastic properties of putative cyclic polymers synthesized by reversible radical recombination polymerization (R3P)," Macromolecules 56, 1013–1032 (2023).
- [12] Fujii, Y., R. Nishikawa, P. Phulkerd, and M. Yamaguchi, "Modifying the rheological properties of polypropylene under elongational flow by adding polyethylene," J. Rheol. 63, 11–18 (2019).
- [13] Gleissle, W., and B. Hochstein, "Validity of the Cox-Merz rule for concentrated suspensions," J. Rheol. 47, 897-910 (2003).
- [14] Kong, D., S. Banik, M. J. San Francisco, M. Lee, R. M. Robertson Anderson, C. M. Schroeder, and G. B. McKenna, "Rheology of entangled solutions of ring-linear DNA blends," Macromolecules 55, 1205–1217 (2022).
- [15] Snijkers, F., and D. Vlassopoulos, "Appraisal of the Cox-Merz rule for well-characterized entangled linear and branched polymers," Rheol. Acta 53, 935–946 (2014).
- [16] Marrucci, G., "Dynamics of entanglements: A nonlinear model consistent with the Cox-Merz rule," J. Non-Newtonian Fluid Mech. 62, 279–289 (1996).
- [17] Ianniruberto, G., and G. Marrucci, "On compatibility of the Cox-Merz rule with the model of Doi and Edwards," J. Non-Newtonian Fluid Mech. 65, 241–246 (1996).
- [18] Mead, D. W., "Analytic derivation of the Cox-Merz rule using the MLD 'toy' model for polydisperse linear polymers," Rheol. Acta 50, 837–866 (2011).
- [19] Doraiswamy, D., A. Mujumdar, I. Tsao, A. Beris, S. Danforth, and A. Metzner, "The Cox-Merz rule extended: A rheological model for concentrated suspensions and other materials with a yield stress," J. Rheol. 35, 647-685 (1991).
- [20] Mujumdar, A., A. N. Beris, and A. B. Metzner, "Transient phenomena in thixotropic systems," J. Non-Newtonian Fluid Mech. 102, 157–178 (2002).

- [21] Booij, H. C., P. Leblans, J. Palmen, and G. Tiemersma-Thoone, "Nonlinear viscoelasticity and the Cox-Merz relations for polymeric fluids," J. Polym. Sci.: Polym. Phys. Ed. 21, 1703–1711 (1983).
- [22] Mas, R., and A. Magnin, "Experimental validation of steady shear and dynamic viscosity relation for yield stress fluids," Rheol. Acta 36, 49–55 (1997).
- [23] Wang, Y., and J. J. Wang, "Shear yield behavior of calcium carbonate-filled polypropylene," Polym. Eng. Sci. 39, 190–198 (1999).
- [24] Raghavan, S. R., and S. A. Khan, "Shear-thickening response of fumed silica suspension under steady and oscillatory shear," J. Colloid Interface Sci. 185, 57–67 (1997).
- [25] Xu, X., X. Tao, C. Gao, and Q. Zheng, "Studies on the steady and dynamic rheological properties of poly(dimethyl-siloxane) filled with calcium carbonate based on superposition of its relative functions," J. Appl. Polym. Sci. 107, 1590–1597 (2008).
- [26] Bayram, G., U. Yilmazer, and N. Orbey, "Viscoelastic properties of suspensions with weakly interacting particle," J. Appl. Polym. Sci. 70, 507–514 (1998).
- [27] Kaully, T., A. Seigmann, and D. Shacham, "Rheology of highly filled natural CaCO₃ composites: II. Effects of solid loading and particle size distribution on rotational rheometry," Polym. Compos. 28, 524–533 (2007).
- [28] Ureña-Benavides, E. E., G. Ao, V. A. Davis, and C. L. Kitchens, "Rheology and phase behavior of lyotropic cellulose nanocrystal suspensions," Macromolecules 44, 8990–8998 (2011).
- [29] Parisi, D., J. Seo, B. Nazari, R. P. Schaake, A. M. Rhoades, and R. H. Colby, "Shear-induced isotropic-nematic transition in poly (ether ether ketone) melts," ACS Macro Lett. 9, 950-956 (2020).
- [30] Vallés, C., R. J. Young, D. J. Lomax, and I. A. Kinloch, "The rheological behaviour of concentrated dispersions of graphene oxide," J. Mater. Sci. 49, 6311–6320 (2014).
- [31] Seo, J., H. Takahashi, B. Nazari, A. M. Rhoades, R. P. Schaake, and R. H. Colby, "Isothermal flow-induced crystallization of polyamide 66 melts," Macromolecules 51, 4269–4279 (2018).
- [32] Parisi, D., S. Costanzo, Y. Jeong, J. Ahn, T. Chang, D. Vlassopoulos, J. D. Halverson, K. Kremer, T. Ge, and M. Rubinstein, "Nonlinear shear rheology of entangled polymer rings," Macromolecules 54, 2811–2827 (2021).
- [33] Larson, R. G., The Structure and Rheology of Complex Fluids (Oxford University, New York, 1999).
- [34] Yu, C., and S. Gunasekaran, "Correlation of dynamic and steady flow viscosities of food materials," Appl. Rheol. 11, 134–140 (2001).
- [35] Ren, J., and R. Krishnamoorti, "Nonlinear viscoelastic properties of layered-silicate-based intercalated nanocomposites," Macromolecules 36, 4443–4451 (2003).
- [36] Domenech, T., R. Zouari, B. Vergnes, and E. Peuvrel-Disdier, "Formation of fractal-like structure in organoclay-based polypropylene nanocomposites," Macromolecules 47, 3417–3427 (2014).
- [37] Yan, Z.-C., S. Costanzo, Y. Jeong, T. Chang, and D. Vlassopoulos, "Linear and nonlinear shear rheology of a marginally entangled ring polymer," Macromolecules 49, 1444–1453 (2016).
- [38] Pyromali, C., Y. Li, F. Zhuge, C.-A. Fustin, E. Van Ruymbeke, and D. Vlassopoulos, "Nonlinear shear rheology of single and double dynamics metal-ligand networks," J. Rheol. 66, 1223–1235 (2022).
- [39] Parisi, D., M. Kaliva, S. Costanzo, Q. Huang, P. J. Lutz, J. Ahn, T. Chang, M. Rubinstein, and D. Vlassopoulos, "Nonlinear rheometry of entangled polymeric rings and ring-linear blends," J. Rheol. 65, 695–711 (2021).
- [40] Jaishankar, A., and G. H. McKinley, "A fractional K-BKZ constitutive formulation for describing the nonlinear rheology of multiscale complex fluids," J. Rheol. 58, 1751–1788 (2014).

- [41] Bricker, J. M., and J. E. Butler, "Oscillatory shear of suspensions of non-colloidal particles," J. Rheol. 50, 711–728 (2006).
- [42] Eckstein, E. C., D. G. Bailey, and A. H. Shapiro, "Self-diffusion of particles in shear flow of a suspension," J. Fluid Mech. 79, 191–208 (1977).
- [43] Leighton, D., and A. Acrivos, "The shear-induced migration of particles in concentrated suspensions," J. Fluid Mech. 181, 415–439 (1987).
- [44] Gadala-Maria, F., and A. Acrivos, "Shear-induced structure in a concentrated suspension of solid spheres," J. Rheol. 24, 799–814 (1980).
- [45] Drazer, G., J. Koplik, B. Khusid, and A. Acrivos, "Deterministic and stochastic behavior of non-Brownian spheres in sheared suspensions," J. Fluid Mech. 460, 307–335 (2002).
- [46] Metzger, B., and J. E. Butler, "Irreversibility and chaos" role of longrange hydrodynamic interactions in sheared suspensions," Phys. Rev. E 82, 051406 (2010).
- [47] Metzger, B., P. Pham, and J. E. Butler, "Irreversibility and chaos: Role of lubrication interactions in sheared suspensions," Phys. Rev. E 87, 052304 (2013).
- [48] Breedveld, V., E. Dvd, R. Jongschaap, and J. Mellema, "Shear-induced diffusion and rheology of noncolloidal suspensions: Time scales and particle displacements," J. Chem. Phys. 114, 5923–5936 (2001).
- [49] Corte, L., P. M. Chaikin, J. P. Gollub, and D. J. Pine, "Random organization in periodically driven systems," Nat. Phys. 4(5), 420–424 (2008).
- [50] Rathinaraj, J. D. J., B. Keshavarz, and G. H. McKinley, "Why the Cox–Merz rule and Gleissle mirror relation work: A quantitative analysis using the Wagner integral framework with a fractional Maxwell kernel," Phys. Fluids 34, 033106 (2022).
- [51] Rathinaraj, J. D. J., G. H. McKinley, and B. Keshavarz, "Incoporating rheological nonlinearity into fractional calculus descriptions of fractal matter and multi-scale complex fluids," Fractal Fract. 5, 174 (2021).
- [52] Lee, J. C.-W., Y.-T. Hong, K. M. Weigandt, E. G. Kelley, H. Kong, and S. A. Rogers, "Strain shifts under stress-controlled oscillatory shearing in theoretical, experimental, and structural perspectives: Application to probing zero-shear viscosity," J. Rheol. 63, 863–881 (2019).
- [53] Lee, J. C.-W., K. M. Weigandt, E. G. Kelley, and S. A. Rogers, "Structure-property relationships via recovery rheology in viscoelastic materials," Phys. Rev. Lett. 122, 248003 (2019).
- [54] Lee, J. C. W., L. Porcar, and S. A. Rogers, "Recovery rheology via rheo-SANS: Application to step strains under out-of-equilibrium conditions," AIChE J. 65, e16797 (2019).

- [55] Donley, G. J., P. K. Singh, A. Shetty, and S. A. Rogers, "Elucidating the G "overshoot in soft materials with a yield transition via a timeresolved experimental strain decomposition," Proc. Natl. Acad. Sci. U.S.A. 117, 21945–21952 (2020).
- [56] Kamani, K., G. J. Donley, and S. A. Rogers, "Unification of the rheological physics of yield stress fluids," Phys. Rev. Lett. 126, 218002 (2021).
- [57] Griebler, J. J., and S. A. Rogers, "The nonlinear rheology of complex yield stress foods," Phys. Fluids 34, 023107 (2022).
- [58] Shim, Y. H., and S. A. Rogers, "Understanding the yielding behavior of graphene oxide colloids via experimental strain decomposition," Phys. Fluids 35, 063117 (2023).
- [59] Shim, Y. H., P. K. Singh, and S. A. Rogers, "Unified interpretation of MAOS responses via experimentally decomposed material functions," J. Rheol. 67, 1141–1158 (2023).
- [60] Donley, G. J., S. Narayanan, M. A. Wade, J. D. Park, R. L. Leheny, J. L. Harden, and S. A. Rogers, "Investigation of the yielding transition in concentrated colloidal systems via rheo-XPCS," Proc. Natl. Acad. Sci. U.S.A. 120, e2215517120 (2023).
- [61] Shi, J., and S. A. Rogers, "The benefits of a formalism built on recovery: Theory, experiments, and modeling," J. Non-Newtonian Fluid Mech. 321, 105113 (2023).
- [62] Griebler, J. J. D., J. Gavin, V. Wisniewski, and S. A. Rogers, "Strain shift measured from stress-controlled oscillatory shear evidence for a continuous yielding transition, and new techniques to determine recovery rheology measures," J. Rheol. (to be published).
- [63] Singh, P. K., J. C.-W. Lee, K. A. Patankar, and S. A. Rogers, "Revisiting the basis of transient rheological material functions: Insights from recoverable strain measurements," J. Rheol. 65, 129–144 (2021)
- [64] Tschoegl, N. W., The Phenomenological Theory of Linear Viscoelastic Behavior: An Introduction (Springer, Berlin, Germany, 1989).
- [65] Matsumoto, A., C. Zhang, F. Scheffold, and A. Q. Shen, G. Wilcrorheological approach for probing the entanglement properties of Boule polyelectrolyte solutions," ACS Macro Lett. 11, 84–90 (2021).
- [66] Pipkin, A. C., Lectures on Viscoelasticity Theory, 2nd ed. (Springer, New York, 1986), Vol. 7.
- [67] White, J. L., "Dynamics of viscoelastic fluids, melt fracture, and the rheology of fiber spinning," J. Appl. Polym. Sci. 8, 2339–2357 (1964).
- [68] Reiner, M., "The Deborah number," Phys. Today 17, 62 (1964).
- [69] Dealy, J., "Weissenberg and Deborah numbers—Their definition and use," Rheol. Bull 79, 14–18 (2010).

21 May 20